A committed fourfold increase in ocean oxygen loss

Andreas Oschlies (aoschlies@geomar.de)
GEOMAR Helmholtz Centre for Ocean Research Kiel https://orcid.org/0000-0002-8295-4013

Physical Sciences - Article

Keywords: ocean deoxygenation, CO2, emissions

Posted Date: October 19th, 2020

DOI: https://doi.org/10.21203/rs.3.rs-87569/v1

Version of Record: A version of this preprint was published at Nature Communications on April 16th, 2021. See the published version at https://doi.org/10.1038/s41467-021-22584-4.

A committed fourfold increase in ocean oxygen loss

Andreas Oschlies[1,2*]

Affiliations:

[1]GEOMAR Helmholtz Centre for Ocean Research Kiel, Düsternbrooker Weg 20, 24105 Kiel, Germany.

[2]Kiel University, 24098 Kiel, Germany.

*e-mail: aoschlies@geomar.de.

Abstract

Less than a quarter of ocean deoxygenation that will ultimately be caused by historical CO_2 emissions is already realized, according to millennial-scale model simulations that assume zero CO_2 emissions from year 2021 onwards. About 80% of the committed oxygen loss occurs below 2000m depth, where a more sluggish overturning circulation will increase water residence times and accumulation of respiratory oxygen demand. According to the model results, the deep ocean will thereby lose more than 10% of its pre-industrial oxygen content even if CO_2 emissions and thus global warming were stopped today. In the surface layer, however, the ongoing deoxygenation will largely stop once CO_2 emissions are stopped. Accounting for the joint effects of committed oxygen loss and ocean warming, metabolic viability representative for marine animals declines by up to 25% over large regions of the deep ocean, posing am unavoidable escalation of anthropogenic pressure on deep-ocean ecosystems.

Introduction

The earth system is not in equilibrium with current levels of atmospheric CO_2 that have experienced an increasingly rapid growth since the beginning of the industrial revolution in mid-19th century, with about half of all anthropogenic CO_2 produced until today emitted during the past 35 years only. Theory and models nevertheless predict that global mean surface temperatures would stop rising further and remain relatively stable for many decades to centuries once CO_2 emissions are stopped[1-3]. This is also implicit in the concept of transient climate response to cumulative CO_2 emissions (TCRE[4,5]), which provides the scientific rationale for relating temperature targets to remaining carbon budgets. Since its mentioning in the Paris Agreement in 2015, the goal of achieving net zero CO_2 emissions in order to stabilize global mean surface temperatures has gained substantial traction in climate politics and scenario development. Accomplishing this goal is sometimes regarded as also stopping the increase in climate damages.

However, even though global-mean surface temperatures are expected to remain stable when CO_2 emissions are stopped, many components of the Earth system will continue to respond to the anthropogenic perturbation with their inherent response timescales and inertia, possibly producing harm long after emissions are stopped. Heat as well as carbon and freshwater will continue to be redistributed among the different planetary reservoirs, in particular atmosphere, land, ocean and cryosphere. The uptake of CO_2 by the ocean essentially gives rise to a slow multi-centennial decline of atmospheric CO_2 and the associated radiative forcing. According to current models, the remaining radiative forcing during this phase of ocean adjustment to the anthropogenic perturbation is closely balanced by oceanic heat uptake[3]. The relative stability of global-mean surface temperatures upon ending CO_2 emissions thus comes at the expense of

50 increasing acidification and warming of the deep ocean[6]. Thermal expansion results in
51 committed sea-level rise[7,8] that will be enhanced further by committed melting of inland
52 ice[9,10]. First studies have looked at committed changes in terrestrial ecosystems[11]. Here
53 we investigate committed changes in marine oxygen levels that are already declining at
54 alarming pace[12,13], and that act, together with warming and acidification, as key
55 stressors on marine ecosystems[14]. Such committed changes will also have to be
56 accounted for when assessing damages caused by anthropogenic CO_2 emissions, even if
57 they materialize well after emissions are stopped and global mean surface air
58 temperatures have stabilized.
59
60 **Committed change in oceanic oxygen inventory**
61 A numerical Earth system model of intermediate complexity[15] that is well calibrated to
62 simulate observed climate properties and oxygen distributions[16] is employed to
63 examine what would happen if CO_2 emissions were stopped end of year 2020. Forced
64 with historical CO_2 emissions until 2010 and emissions corresponding to the Reference
65 Concentration Pathway (RCP) 8.5 high-emission scenario[17] until year 2020, the model
66 simulates atmospheric CO_2 levels of 411 μatm and global annual-mean surface air
67 temperatures 1.03°C above pre-industrial in year 2020, in agreement with observations.
68 After emissions are stopped end of 2020, simulated surface air temperatures increase by
69 another 0.04°C within 7 years before slowly leveling off at about 0.01°C above year-2020
70 temperatures towards the end of the 21st century and staying within +-0.02°C at this
71 level until year 2650 (Figure 1a).
72
73 A major deep-convection event in the Southern Ocean after year 2650 sets off a
74 substantial release of heat and CO_2 from the ocean to the atmosphere and surface air

temperatures rise abruptly by 0.4°C within 50 years. Such deep convection events have been found in a number of climate models under equilibrium[18] and continued CO_2 emission pathways[19]. In the zero-emission commitment scenario investigated here, the combination of stabilized surface temperatures with warming subsurface waters of North Atlantic origin eventually renders stratification unstable in the Southern Ocean, triggering deep convective overturning after year 2650. This leads to enhanced ventilation of the deep ocean from the south and an eventual re-oxygenation of the deep ocean also seen under continued emissions[20,21]. Simulated globally-averaged ocean temperature increases from a pre-industrial value of 3.07°C to 3.23°C in year 2020 and shows continued warming to 3.70°C until year 2650, followed by a subsequent gradual cooling to 3.56°C in year 3000 (Figure 1a).

There is substantial uncertainty, requiring further study, about the relative roles in heat and fresh-water forcings and the degree of realism in simulated Southern Ocean processes in current climate models[19]. Therefore, we here focus our analysis of committed changes on the time until year 2650, by which all model properties show an asymptotic adjustment to the stabilized surface temperatures. For the present study, we regard subsequent effects associated with the still poorly understood enigmatic deep-convection event in the model's Southern Ocean as a plausible but as yet uncertain tipping element in the climate system.

The stabilization of global-mean surface air temperatures after emissions stop end of year 2020 (Figure 1a) is a result of the ocean continuing to take up heat and CO_2 (ref.3) (Figure 1b). The committed future uptake of CO_2 from the atmosphere (720 Gt CO_2 until 2650) is larger than all the CO_2 the ocean has taken up until 2020 (634 Gt CO_2), whereas

the committed future ocean heat uptake until year 2650 (2.7×10^{24} J) is even three times as large as the heat taken up until year 2020 (0.9×10^{24}), leading to another 16 cm of unavoidable thermobaric global sea level rise. The simulated oceanic oxygen inventory declines by 5.0 Pmol O_2 (1.8 %) from pre-industrial year 1800 to 2020. This is consistent with the decline found in other Earth system models[22], but somewhat slower than inferred from observations that suggest a 4.8 +- 2.1 Pmol decline between 1960 and 2010 alone[12]. The simulated oxygen decline continues for several hundred years after stopping emissions in 2020 and asymptotically reaches a total loss of 20.3 Pmol O_2 until year 2650 (Figure 1b), corresponding to 7.4 % of the pre-industrial oxygen inventory. Similar to the magnitude of the committed heat uptake, the committed oxygen loss is more than three times as large as the oxygen loss that has occurred until the emissions stop end of year 2020.

There is a close proportionality of global ocean heat gain and oxygen loss until year 2650 (extended data Figure S1) with a ratio of 5.7 +-0.9 nmol J^{-1}, consistent with earlier observational estimates of thermocline oxygen losses[23]. The total oxygen loss is 3 to 4 times larger than the direct solubility effect of warming shown in form of an abiotic oxygen tracer in Figure 1b. Only the Southern Ocean deep convection event after year 2650 breaks this proportionality by bringing large volumes of deep waters with a high share of accumulated respiratory oxygen deficit into contact with the atmosphere and thereby increasing the marine oxygen inventory without dominant changes to the solubility-driven oxygen component (Figure 1b).

Patterns and processes

Despite the tight correlation of global-ocean heat uptake and oxygen loss, regional patterns of warming and deoxygenation are very different. Until year 2020, zonally averaged ocean warming is largest in the mid and low-latitude near-surface waters (Figure 2c) with vertically averaged warming being most prominent along the western boundary of the North Atlantic (Figure 2a) where deep western boundary currents transport warming North Atlantic Deep Water southward. Oxygen loss, on the other hand, is most pronounced in the deep water formation regions in the Southern Ocean and North Atlantic (Figures 2b,d). Similar to many other models, there is even a slight oxygen gain in the tropical thermocline that is in conflict with observations and deemed attributable to the model's failure to correctly reproduce temporal changes in the wind field[16].

The committed ocean warming between years 2020 and 2650 by about half a degree Celsius is relatively homogeneous in the subsurface waters (Figure 2g), but largest in the North Atlantic, where the overturning circulation ensures rapid spreading of warmer waters throughout the basin (Figure 2e). Surface waters in immediate contact with the stabilized surface air temperatures show very little change in both temperatures and oxygen concentrations. There are, however, considerable regional differences in the magnitude of committed oxygen changes in the ocean interior. Committed oxygen loss is largest around Antarctica and in bottom and deep waters throughout the world ocean (Figures 2f,h), where oxygen concentrations decline by typically 30 mmol/m^3. The Atlantic shows little changes and, in some regions, even an oxygen increase due to the slowly increasing ventilation via the formation of North Atlantic Deep Water and the strengthening meridional overturning circulation (contours in Figure 2h).

The different patterns of committed warming and deoxygenation can be explained by the direct impact of biological respiration and water residence times on interior-ocean oxygen concentrations, but not on temperatures. While the solubility-driven oxygen changes tightly follow the patterns of ocean warming (Figure S2a,b), the more sluggish overturning circulation leads to increases in simulated bottom and deep-water ideal age by several hundred years by year 2650 (Figure S3). The export of organic matter out of the surface ocean increases by about 4% between year 2020 and 2650 (Figure S4). Since remineralization rates increase with increasing temperatures, remineralization tends to move to slightly shallower depths under ocean warming. The combined effect of an increase in export production and a shoaling of remineralization is little committed change in respiratory oxygen consumption in the deep ocean (Figure S5). According to these model results, the committed loss of marine oxygen is predominantly caused by changes in ocean physics.

While ocean warming directly determines the solubility-driven oxygen loss, which, in the model, maintains a roughly 30% share of total deoxygenation all the way to year 2650 (Figure 1b), the majority of the committed oxygen loss is a result of the increase in water residence time particularly in the deep Southern Ocean and the North Pacific (Figure S3c). These waters are relatively well oxygenated (O_2 > 150 mmol m^{-3}), whereas low oxygen waters, sometimes called hypoxic (O_2 < 70 mmol m^{-3}) or suboxic (O_2 < 5 mmol m^{-3}), are generally found at depths shallower than a few hundred meters. Between years 2020 and 2650, the volume of hypoxic and suboxic waters shows only a relatively small and steady committed increases by 8% and 15%, respectively. This is small compared to the 150% increase seen in an extended multi-millennial RCP 8.5 scenario[20].

Implications

Committed oxygen loss generates the largest decline in oxygen concentrations in deep waters (Figure 2h) at oxygen concentrations relatively high compared to oxygen minimum zones typically located at a depth of a few hundred meters. Largest committed volumetric changes are simulated for waters with oxygen concentrations in the range between 230 and 270 mmol m^{-3}, that lose more than half of their volume between years 2020 and 2650, on the expense of volume gains at lower oxygen classes between 200 and 230 mmol m^{-3} and 130 to 180 mmol m^{-3} (Figure 3). Though relatively little is known about deep-ocean ecosystems and their sensitivity to oxygen change, it is likely that animals have evolved to optimally exploit ambient oxygen levels[25]. Thus, any loss of oxygen is expected to reduce habitats of individual species. The rate of oxygen decline is small, on average about 5 mmol m^{-3} per 100 years until year 2650, but, according to the model, unavoidable even if CO_2 emissions were stopped end of year 2020. The generally low natural variability in the properties of deep water masses may make their ecosystems more vulnerable to oxygen changes than near-surface systems that are naturally exposed to large seasonal and interannual oxygen fluctuations. The speed of model-derived anthropogenic warming relative to natural variability has recently been identified to be largest in mid and deep waters[26]. This would directly translate to the solubility-driven component of oxygen decline. Given that the solubility contributes less (<20%) than average (30%) to total oxygen loss in the deep waters (Figure S2c), the velocity of oxygen change can be expected to be even larger than that of warming.

A metabolic index[27] defined as the ratio of O_2 supply to the temperature-dependent resting O_2 demand of an organism (see methods) and indicator of metabolically viable

marine environments, declines by 10% to 25% over much of the deep ocean below 2000 m between year 2020 and 2650 (Figure 4). Almost all of this reduction in the metabolic index results from oxygen decline. With species generally evolved such that their physiological capacity for oxygen supply matches the maximum evolved demand at the available oxygen pressure[25,28], an oxygen decline of this magnitude can be expected to have substantial impacts on the still poorly explored deep ocean fauna. This calls for efforts to explore the baseline of these systems before the unavoidable change will hit. A future recovery of oxygen concentrations as predicted by climate models after many hundred years of warming-induced deep-ocean deoxygenation[20,21] will come too late for many organisms. If RCP 8.5 CO_2 emissions continue until year 2100 and decrease linearly to zero in year 2300 as assumed in earlier studies with the same model[20], the marine oxygen loss will be even 2.5 times higher until year 2650.

On a positive note, present-day oxygen minimum zones in the upper few hundred meters experience, on average, only little change once CO_2 emissions are stopped (Figures 2h and 3b). This indicates that rapid emission reduction can halt the increasing threat of deoxygenation in the upper ocean that holds much of the known biodiversity and provides the main ocean ecosystem services deemed societally relevant. For deep waters of the ocean, however, there is little hope that even an immediate stop of CO_2 emissions will avert a drastic decline in oxygen concentrations, significantly reducing metabolically viable habitats of deep-sea animals. The deep ocean appears committed to turning into an as yet unrecognized area where the slogan of the American Lung Association “If you can’t breathe, nothing else matters” will become reality for centuries to come.

Data availability

The data presented in the paper are from model simulations described in the Methods. The data will be made available before publication and can also be obtained from the author upon reasonable request.

Code availability

All model and analysis code will be made available before publication.

Acknowledgement

The author thanks the members of the Marine Biogeochemical Research Unit at GEOMAR for fruitful discussions and in particular Iris Kriest for essential help with the ferret analysis software.

Author contributions: AO designed and carried out the model runs and wrote the paper.

Competing interests: The author declares no competing interests.

References

1. Plattner, G. K., R. Knutti, F. Joos, T. F. Stocker, W. von Bloh, V. Brovkin, D. Cameron, E. Driesschaert, S. Dutkiewicz, M. Eby, N. R. Edwards, T. Fichefet, J. C. Hargreaves, C. D. Jones, M. F. Loutre, H. D. Matthews, A. Mouchet, S. A. Müller, S. Nawrath, A. Price, A. Sokolov, K. M. Strassmann, and A. J. Weaver. Long-term climate commitments projected with climate–carbon cycle models. Journal of Climate, 21, 2721–2751, 2008.

2. Matthews. H. D. and A. J. Weaver. Committed climate warming. Nature Geoscience, 3, 142–143, 2010.
3. Williams, R. G., V. Roussenov, T. L. Frölicher, and P. Goodwin. Drivers of continued surface warming after cessation of carbon emissions. Geophysical Research Letters, 44, 10,633–10,642, 2017.
4. Allen, M. R., D. J. Frame, C. Huntingford, C. D. Jones, J. A. Lowe, M. Meinshausen, and N. Meinshausen. Warming caused by cumulative carbon emissions towards the trillionth tonne. Nature, 458, 1163– 1166, 2009.
5. MacDougall, A. H. The transient response to cumulative CO2 emissions: a review. Current Climate Change Reports, 2, 39–47, 2016.
6. Frölicher R. L. and F. Joos. Reversible and irreversible impacts of greenhouse gas emissions in multi- century projections with the NCAR global coupled carbon cycle-climate model. Climate Dynamics, 35, 1439–1459, 2010.
7. NGillett, N. P., V. K. Arora, K. Zickfeld, S. J. Marshall, and W. J. Merryfield. Ongoing climate change following a complete cessation of carbon dioxide emissions. Nature Geoscience, 4, 83–87, 2011.
8. Mengel, M., A. Nauels, J. Rogelj, and C.-F. Schleussner. Committed sea-level rise under the Paris Agreement and the legacy of delayed mitigation action. Nature Communications, 9, 601, 2018.
9. Clark, P. U., J. D. Shakun, S. A. Marcott, A. C. Mix, M. Eby, S. Kulp, A. Levermann, G. A. Milne, P. L. Pfister, B. D. Santer, D. P. Schrag, S. Solomon, T. F. Stocker, B. H. Strauss, A. J. Weaver, R. Winkelmann, D. Archer, E. Bard, A. Goldner, K. Lambeck, R. T. Pierrehumbert, and G.-K. Plattner. Consequences of twenty-first-century policy for multi-millennial climate and sea-level change. Nature Clim. Change, 6, 360–369, 2016.

10. Marzeion, B., G. Kaser, F. Maussion, and N. Champollion. Limited influence of climate change mitigation on short-term glacier mass loss. Nature Climate Change, 8, 305–308, 2018.
11. Jones, C., J. Lowe, S. Liddicoat, and R. Betts. Committed terrestrial ecosystem changes due to climate change. Nature Geosci, 2, 484–487, 2009.
12. Schmidtko, S., L. Stramma, and M. Visbeck. Decline in global oceanic oxygen content during the past five decades. Nature, 542, 335–339, 2017.
13. Breitburg, D., L. A. Levin, A. Oschlies, M. Grégoire, F. P. Chavez, D. J. Conley, V. Garçon, D. Gilbert, D. Gutiérrez, K. Isensee, G. S. Jacinto, K. E. Limburg, I. Montes, S. W. A. Naqvi, G. C. Pitcher, N. N. Rabalais, M. R. Roman, K. A. Rose, B. A. Seibel, M. Telszewski, M. Yasuhara, and J. Zhang. Declining oxygen in the global ocean and coastal waters. Science, 359, 2018.
14. Gruber, N. Warming up, turning sour, losing breath: Ocean biogeochemistry under global change. Philosophical Transactions of the Royal Society of London A: Mathematical, Physical and Engineering Sciences, 369, 1980–1996, 2011.
15. Weaver, A. J. et al. The UVic earth system climate model: model description, climatology, and applications to past, present and future climates. Atmosphere-Ocean 39, 361–428, 2001.
16. Oschlies, A., O. Duteil, J. Getzlaff, W. Koeve, A. Landolfi, and S. Schmidtko. Patterns of deoxygenation: sensitivity to natural and anthropogenic drivers. Philosophical Transactions of the Royal Society A: Mathematical, Physical and Engineering Sciences, 375, 2017.
17. Riahi, K., S. Rao, V. Krey, C. Cho, V. Chirkov, G. Fischer, G. Kindermann, N. Nakicenovic, and P. Rafaj. RCP 8.5 – a scenario of comparatively high greenhouse gas emissions. Climatic Change, 109, 33, 2011.

18. Meissner, K. J., M. Eby, A. J. Weaver, and O. A. Saenko. CO2 threshold for millennial-scale oscillations in the climate system: implications for global warming scenarios. Climate Dynamics, 30, 161, 2007.
19. de Lavergne, C., J. B. Palter, E. D. Galbraith, R. Bernardello, and I. Marinov. Cessation of deep convection in the open Southern Ocean under anthropogenic climate change. Nature Clim. Change, 4, 278–282, 2014.
20. Oschlies, A., W. Koeve, A. Landolfi, and P. Kähler. Loss of fixed nitrogen causes net oxygen gain in a warmer future ocean. Nature Communications, 10, 2805, 2019.
21. Frölicher, T. L., M. T. Aschwanden, N. Gruber, S. Jaccard, J. P. Dunne, and D. Paynter. Contrasting upper and deep ocean oxygen response to protracted global warming. Global Biogeochemical Cycles, 34, e2020GB006601, 2020.
22. Bopp, L., L. Resplandy, J. C. Orr, S. C. Doney, J. P. Dunne, M. Gehlen, P. Halloran, C. Heinze, T. Ilyina, R. Séférian, J. Tjiputra, and M. Vichi. Multiple stressors of ocean ecosystems in the 21st century: projections with CMIP5 models. Biogeosciences, 10, 6225–6245, 2013.
23. RKeeling R. F. and H. E. Garcia. The change in oceanic O2 inventory associated with recent global warming. Proceedings of the National Academy of Sciences, 99, 7848–7853, 2002.
24. Garcia, H. E., K. Weathers, C. R. Paver, I. Smolyar, T. P. Boyer, R. A. Locarnini, M. M. Zweng, A. V. Mishonov, O. K. Baranova, D. Seidov, and J. R. Reagan, 2018. World Ocean Atlas 2018, Volume 3: Dissolved Oxygen, Apparent Oxygen Utilization, and Oxygen Saturation. A. Mishonov Technical Ed.; NOAA Atlas NESDIS 83, 38 pp.
25. Seibel B. A. and C. Deutsch. Oxygen supply capacity in animals evolves to meet maximum demand at the current oxygen partial pressure regardless of size or temperature. The Journal of Experimental Biology, 223, jeb210492, 2020.

26. Brito-Morales, I., D. S. Schoeman, J. G. Molinos, M. T. Burrows, C. J. Klein, N. Arafeh-Dalmau, K. Kaschner, C. Garilao, K. Kesner-Reyes, and A. J. Richardson. Climate velocity reveals increasing exposure of deep-ocean biodiversity to future warming. Nature Climate Change, 10, 576-581,2020.
27. Deutsch, C., A. Ferrel, B. Seibel, H.-O. Pörtner, and R. B. Huey. Climate change tightens a metabolic constraint on marine habitats. Science, 348, 1132–1135, 2015.
28. Deutsch, C., J. L. Penn, and B. Seibel. Metabolic trait diversity shapes marine biogeography. Nature, 585, 557–562, 2020.

Methods

The University of Victoria (UVic) Earth System Climate Model[15], version 2.8, is employed in the configuration described by ref.20. The ocean component is a fully three-dimensional primitive-equation model with nineteen levels in the vertical ranging from 50 m near the surface to 500 m in the deep. It contains a simple marine ecosystem model including the two major nutrients nitrate and phosphate and two phytoplankton classes, nitrogen fixers and other phytoplankton, the former being limited by phosphate only. The micronutrient iron is not explicitly included in the model, which nevertheless achieves a reasonable fit to observed biogeochemical tracer distributions for the tuned biological parameters and mixing parameterizations[29]. For the assumed molar stoichiometry of C:N:P:$-O_2$ = 112:16:1:169.6, organic matter is degraded by aerobic remineralization ($-O_2$:PO_4 = 169.6) as long as sufficient dissolved oxygen is available. In regions where oxygen concentrations fall below a threshold of 5 mmol O_2 m^{-3}, nitrate is used as electron acceptor (denitrification, $-NO_3$:PO_4 = 119.68, see ref.30). No other

electron acceptors are simulated and remineralization stops whenever nitrate runs out, which does not happen in the model runs used here.

The ocean component is coupled to a single-level energy-moisture balance model of the atmosphere, a dynamic-thermodynamic sea ice component and a terrestrial vegetation and carbon-cycle component. Continental ice sheets are prescribed and kept fixed in the present configuration. All model components use a common horizontal resolution of 1.8° latitude times 3.6° longitude. The current model version does not consider any fluxes across the water-sediment interface and also does not account for fluxes related to weathering on land. Oceanic phosphorus is thus strictly conserved. Because the atmosphere contains about a hundred times as much oxygen as the ocean, any feedback of marine oxygen changes on atmospheric oxygen is neglected as in earlier studies (e.g. ref.20).

The model is spun up for more than ten thousand years under preindustrial atmospheric CO_2 and forced with historical CO_2 emissions from year 1765 until 2010 and emissions corresponding to the Reference Concentration Pathway (RCP) 8.5 high-emission scenario[17] until year 2020. Solar forcing follows astronomical parameters and the atmospheric composition is assumed constant except for CO_2. In the idealized model scenario aimed at studying the zero emissions commitment[31], CO_2 emissions are abruptly stopped at the end of year 2020 and kept zero thereafter until the end of the model run in year 3000. In model simulations that also stop emissions of non-CO_2 greenhouse gases and aerosols, the climate warms for a few years in response to the negative radiative forcing associated with the rapid decline of short-lived atmospheric aerosols, before a more gradual cooling sets in due to the decline in non-CO_2 greenhouse

gases. After about a century, the response in such models is largely dominated by the long-lived CO_2 and global mean temperatures converge to those obtained under elimination of CO_2 emissions alone[32]. Similar configurations of this model have been employed in earlier investigations of committed warming[33] and committed sea-level rise[34].

In the configuration employed here, eutrophication via runoff or atmospheric deposition of nutrients is not considered, and ocean deoxygenation is thus entirely caused by effects related to anthropogenic CO_2 emissions. Anthropogenic effects of atmospheric nitrogen deposition have been studied elsewhere and found small compared to the ongoing warming-driven deoxygenation (e.g. refs. 35,36) as a result of stabilizing feedbacks in the nitrogen cycle[37].

The metabolic index Φ (ref.27) is defined as the ratio of O_2 supply to the temperature-dependent resting O_2 demand of an organism, and it combines temperature and pO_2 as indicators of metabolically viable marine environments. Here, only changes of Φ are considered[37] employing the scripts provided by ref.39:

$$\frac{\Delta\Phi(t,t_0)}{\Phi(t_0)} = \frac{pO_2(t)}{pO_2(t_0)} \exp\left(\frac{E_0}{k_B}\left[\frac{1}{T(t)} - \frac{1}{T(t_0)}\right]\right) - 1$$

Here, E_0 describes the temperature sensitivity of the resting metabolic rate, which is different for different species. Here, the species average of ref.28 is taken (E_0 = 0.69 eV). Parameter k_B is the Boltzmann constant, pO_2 partial pressure of oxygen.

396 **References**

397 29. Schmittner, A., Oschlies, A., Matthews, H. D. & Galbraith, E. D. Future changes in
398 climate, ocean circulation, ecosystems, and biogeochemical cycling simulated for
399 a business-as-usual CO_2 emission scenario until year 4000 AD. Glob. Biogeochem.
400 Cycles 22, GB1013, 2008.
401 30. Paulmier, A., Kriest, I. and Oschlies, A. Stoichiometries of remineralisation and
402 denitrification in global biogeochemical ocean models. Biogeosciences 6, 923–
403 935, 2009.
404 31. Rogelj, J., P. M. Forster, E. Kriegler, C. J. Smith, and R. Séférian. Estimating and
405 tracking the remaining carbon budget for stringent climate targets. Nature, 571,
406 335–342, 2019.
407 32. Zickfeld, K., M. Eby, A. J. Weaver, K. Alexander, E. Crespin, N. R. Edwards, A. V.
408 Eliseev, G. Feul- ner, T. Fichefet, C. E. Forest, P. Friedlingstein, H. Goosse, P. B.
409 Holden, F. Joos, M. Kawamiya, D. Kicklighter, H. Kienert, K. Matsumoto, I. I.
410 Mokhov, E. Monier, S. M. Olsen, J. O. P. Pedersen, M. Perrette, G. Philippon-
411 Berthier, A. Ridgwell, A. Schlosser, T. Schneider Von Deimling, G. Shaffer, A.
412 Sokolov, R. Spahni, M. Steinacher, K. Tachiiri, K. S. Tokos, M. Yoshimori, N. Zeng,
413 and F. Zhao. Long-term climate change commitment and reversibility: An EMIC
414 intercomparison. Journal of Climate, 26,5782–5809, 2013.
415 33. Ehlert, D. and K. Zickfeld. What determines the warming commitment after
416 cessation of CO_2 emissions? Environ. Res., Lett., 12, 015002, 2017.
417 34. Ehlert D. and K. Zickfeld. Irreversible ocean thermal expansion under carbon
418 dioxide removal. Earth System Dynamics, 9, 197–210, 2018.

35. Krishnamurthy, A., J. K. Moore, C. S. Zender, and C. Luo. Effects of atmospheric inorganic nitrogen deposition on ocean biogeochemistry. Journal of Geophysical Research: Biogeosciences, 112, G02019, 2007.
36. Landolfi, A., C. J. Somes, W. Koeve, L. M. Zamora, and A. Oschlies. Oceanic nitrogen cycling and N O flux perturbations in the Anthropocene. Global Biogeochemical Cycles, 31, 1236–1255, 2017.
37. Somes, C. J., A. Landolfi, W. Koeve, and A. Oschlies. Limited impact of atmospheric nitrogen deposition on marine productivity due to biogeochemical feedbacks in a global ocean model. Geophysical Research Letters, 43, 4500–4509, 2016.
38. Battaglia G. and F. Joos. Hazards of decreasing marine oxygen: the near-term and millennial-scale benefits of meeting the Paris climate targets. Earth System Dynamics, 9, 797–816, 2018.
39. Hofmann, A. F., E. T. Peltzer, P. M. Walz, and P. G. Brewer. Hypoxia by degrees: Establishing definitions for a changing ocean. Deep Sea Research Part I: Oceanographic Research Papers, 58, 1212–1226, 2011.

Figures

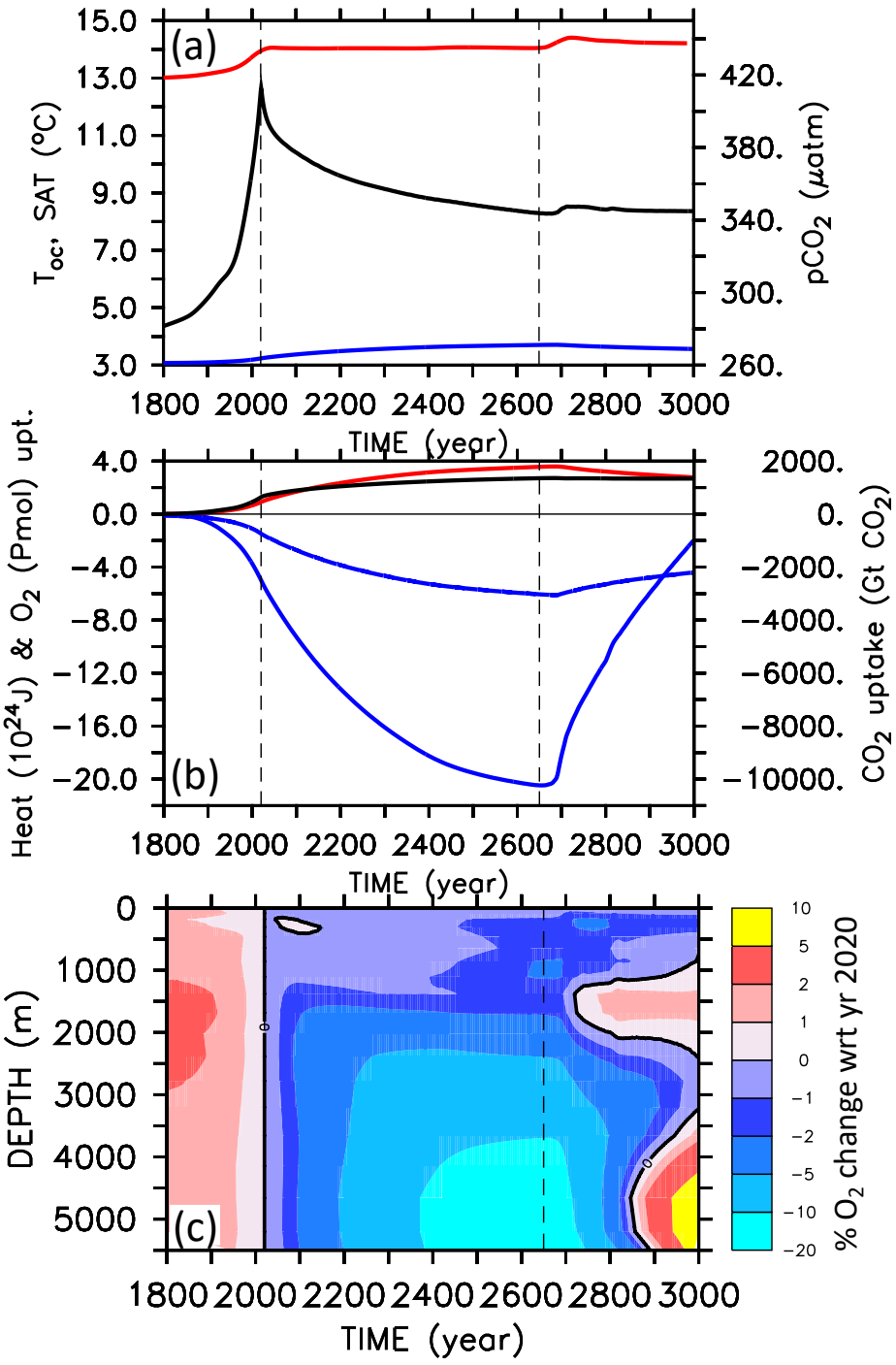

Figure 1 (a) Simulated global annual-mean surface air temperature (SAT, red), atmospheric pCO_2 (black) and ocean mean temperature (Toc, blue). (b) Change in ocean inventory of heat (red), CO_2 (black), dissolved oxygen (O2, blue) and its abiotic (solubility) component (abiotO2, dashed blue) with respect to year 1800.

(c) Change in laterally integrated oxygen concentration as a function of depth over time, expressed in percent change relative to year 2020. Vertical dashed black lines mark then end of year 2020 when emissions stop and the end of the evaluation period in year 2650, just before the onset of the Southern Ocean deep convection event.

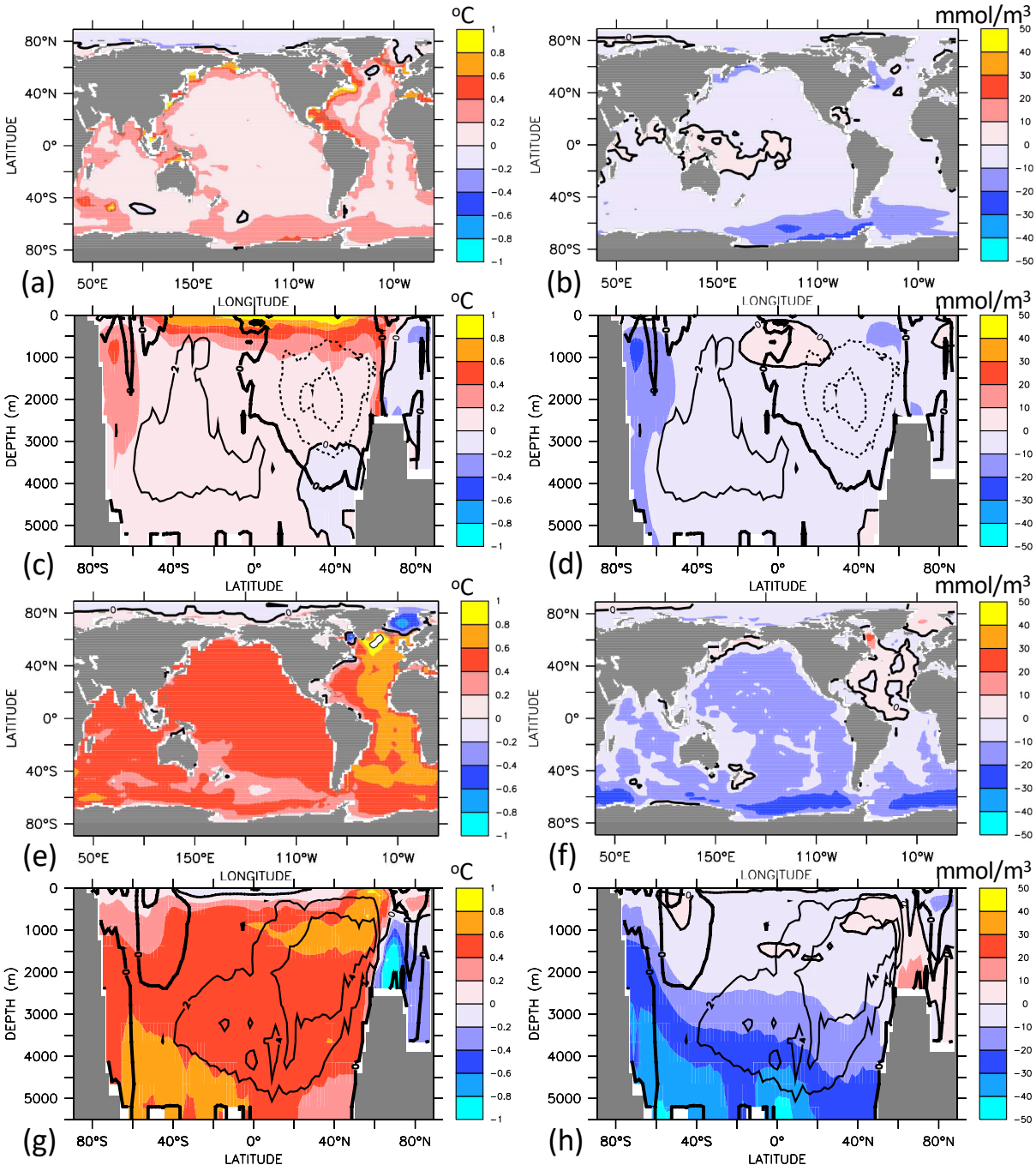

Figure 2: Simulated change in temperature (left column) and oxygen (right column). (a,b) vertically averaged difference year 2020 minus 1800, (c,d) zonally averaged year 2020 minus year 1800, (e,f) vertically averaged difference year 2650 minus 2020, and (g,h) zonally averaged difference year 2650 minus 2020. Contour lines indicate changes in the zonally averaged overturning stream function, with 2 Sv spacing of the iso-contours.

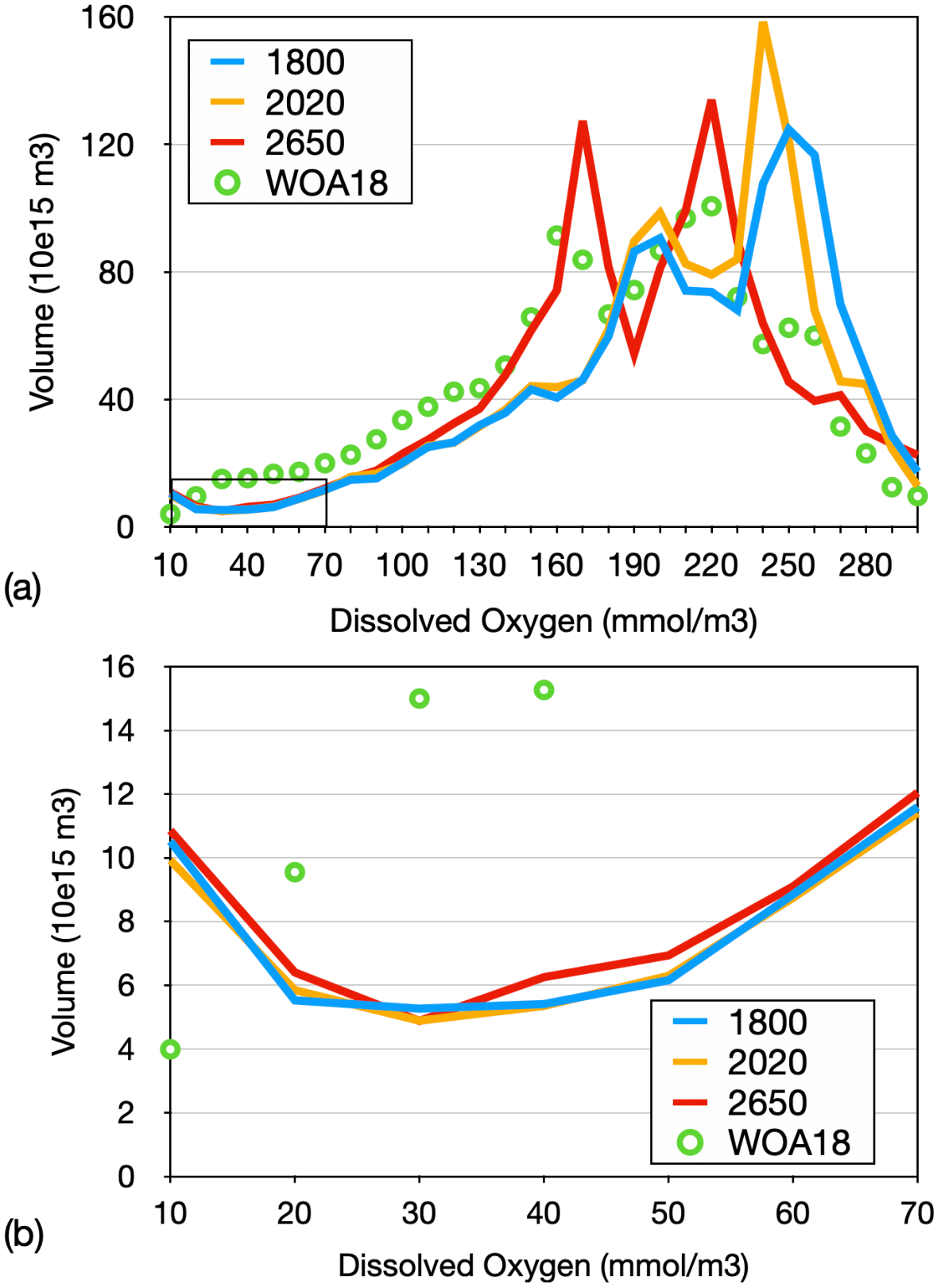

454

455 Figure 3. Simulated water volume (10^{15} m^3) binned according to oxygen concentration

456 with bin width of 10 mmol m^{-3}. Blue refers to year 1800, orange to year 2020 and red to

457 year 2650. Circles refer to the data of the World Ocean Atlas 2018 (ref.24).

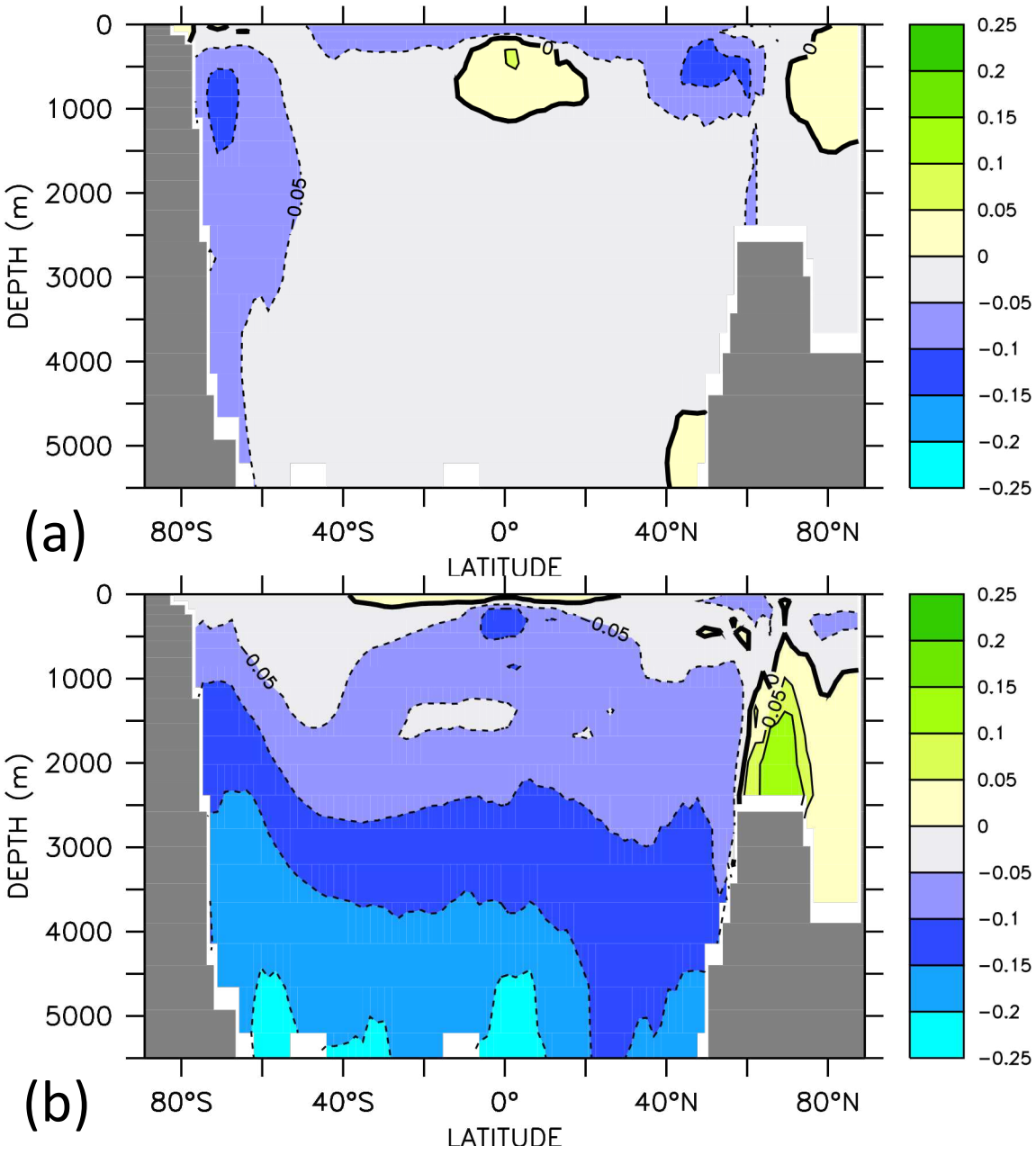

458

459 Figure 4. Zonally averaged relative changes in the metabolic index Φ (see text) for (a)

460 year 2020 with respect to year 1800, (b) year 2650 with respect to year 2020.

Extended Data

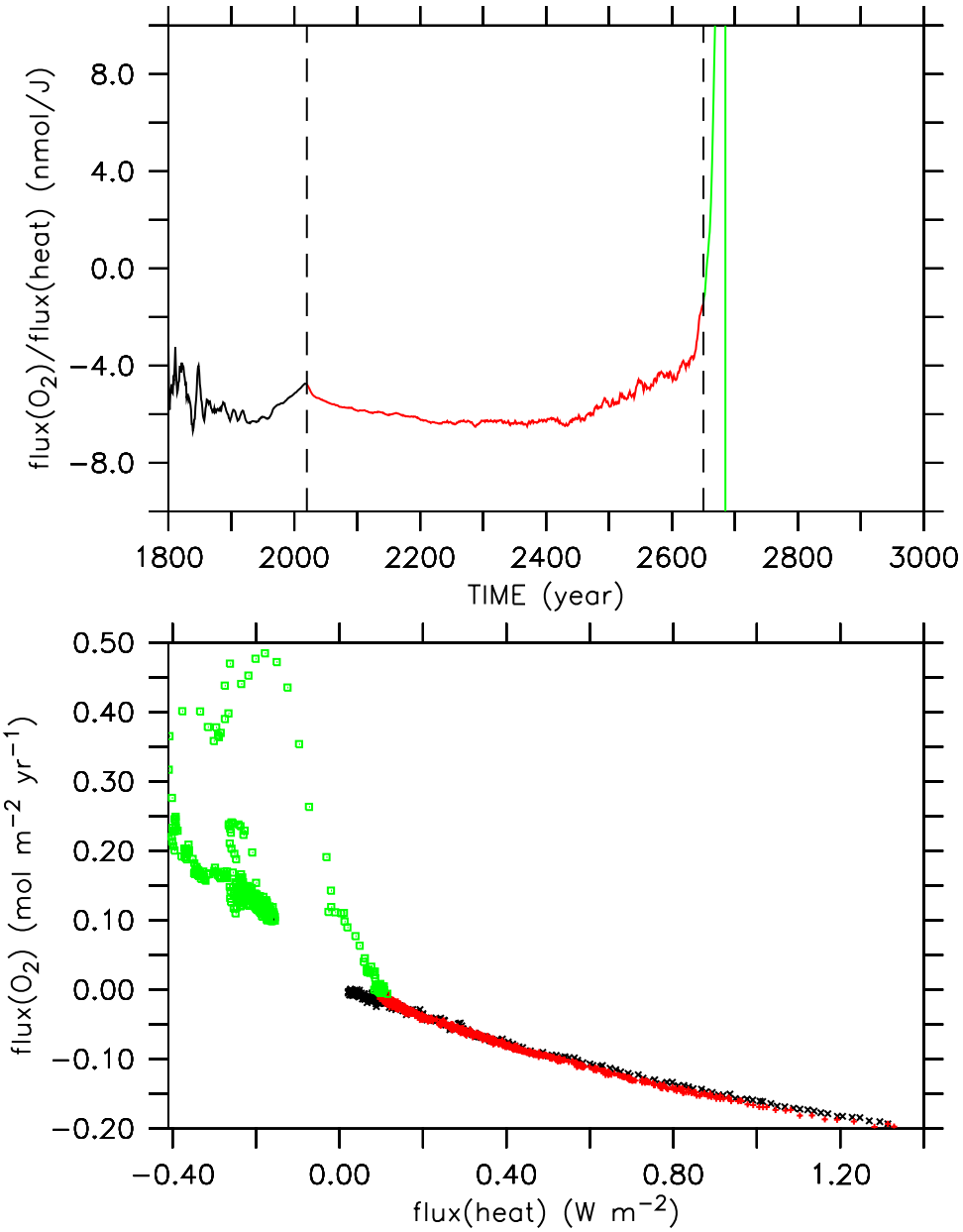

Figure S1: Top: Ratio of simulated annual-mean global air-sea fluxes of oxygen and heat, with positive fluxes directed into the ocean. Color code refers to the periods 1800-2020 (black), 2021-2650 (red), and 2651-3000 (green). Bottom: Annual mean air-sea oxygen fluxes versus heat fluxes.

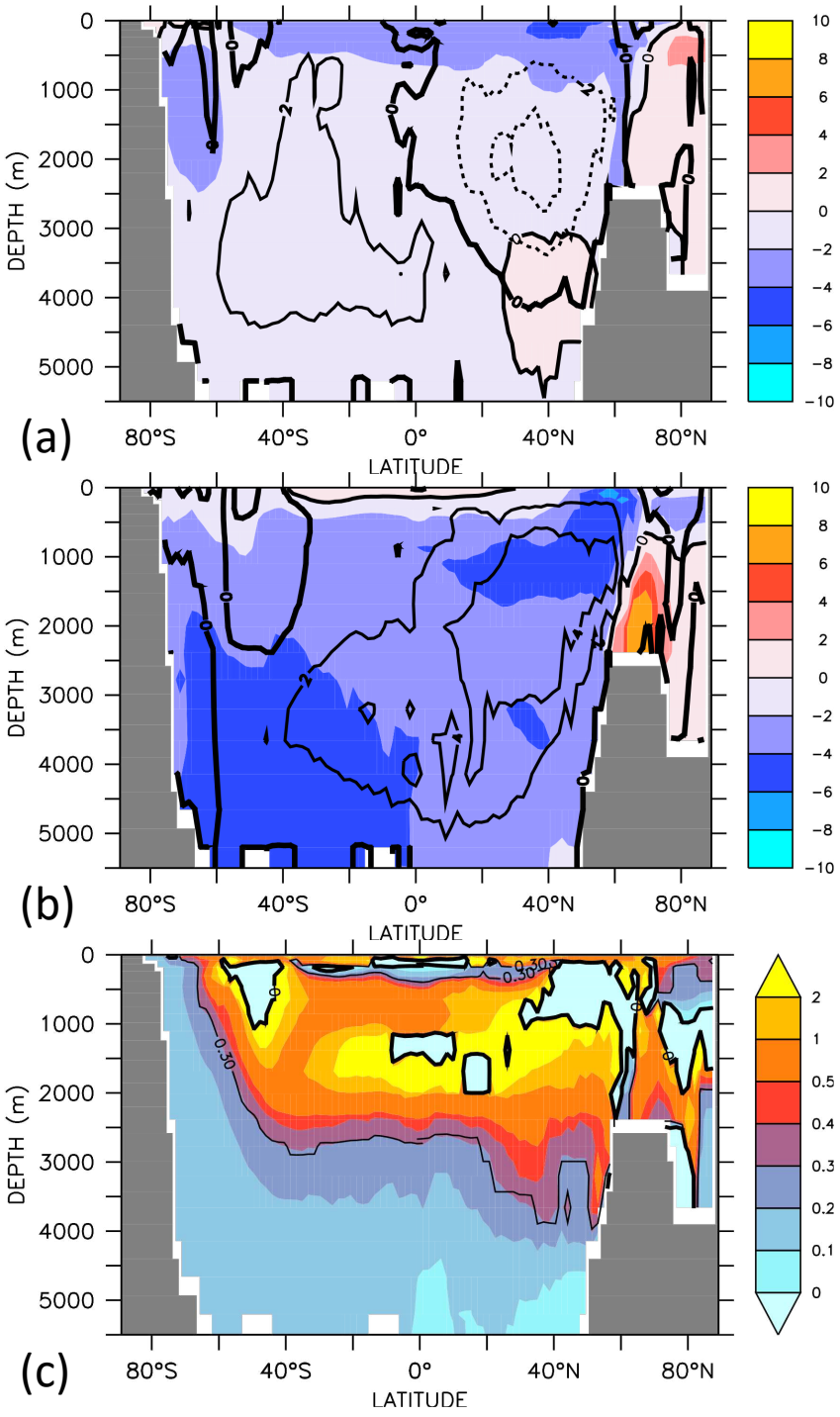

Figure S2. Zonally averaged change in the abiotic oxygen tracer (a) year 2020 minus year 1800, (b) year 2650 minus year 2020. Units are mmol/m^3. Contours are changes in the overturning stream function (units Sv, with increments of 2 Sv) over the same time intervals. (c) Ratio of zonally averaged change in abiotic oxygen to zonally averaged change in oxygen (year 2650 minus year 2020). The 0.3 isoline indicates the global mean ratio.

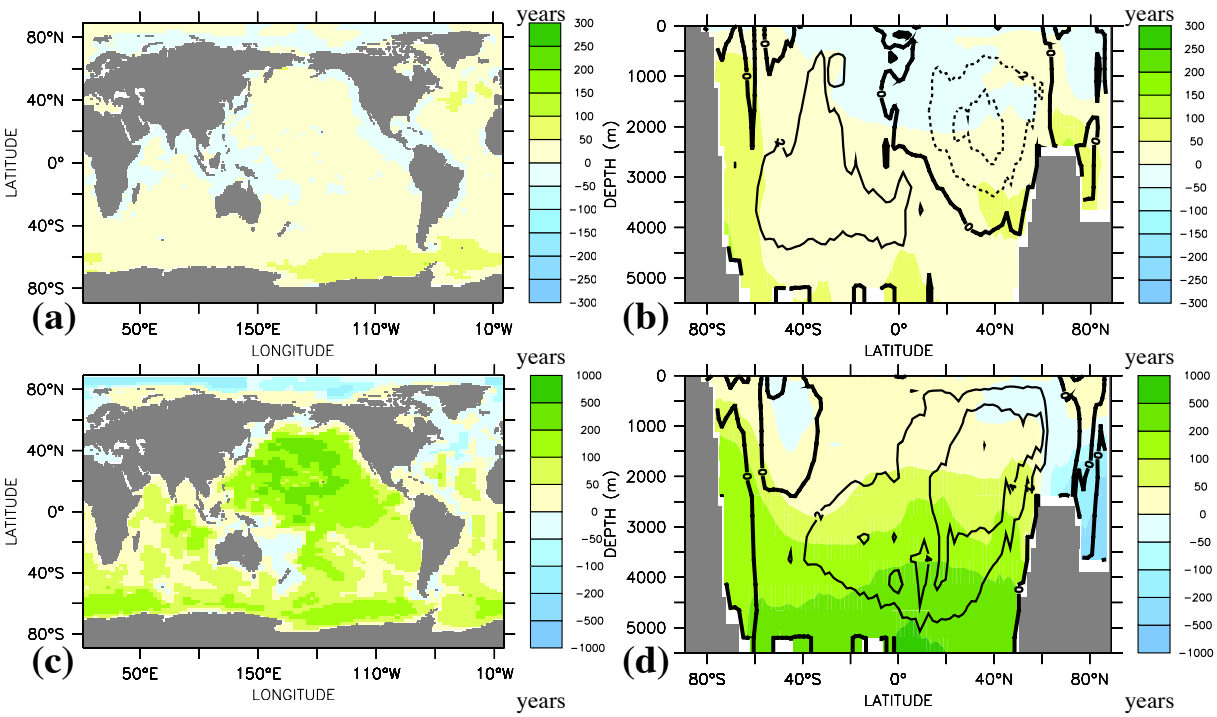

Figure S3: Changes in vertically and zonally averaged water age for (a, b) year 2020 minus year 1800, (c, d) year 2650 minus year 2020. Contours in (b) and (d) are changes in the overturning stream function (units Sv, with increments of 2 Sv) over the same time intervals.

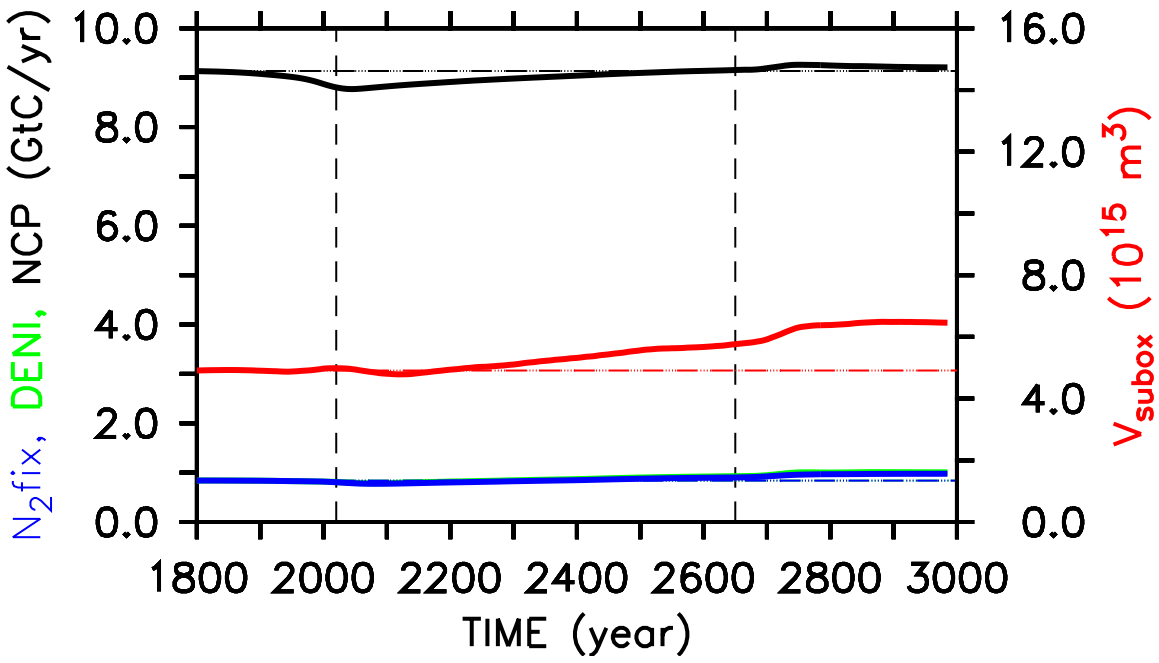

Figure S4: Temporal evolution of globally integrated Net Community Production (NCP, black), denitrification (green), almost identical to nitrogen fixation (blue), and the volume of waters with oxygen concentrations lower than 5 mmol m^{-3} (red).

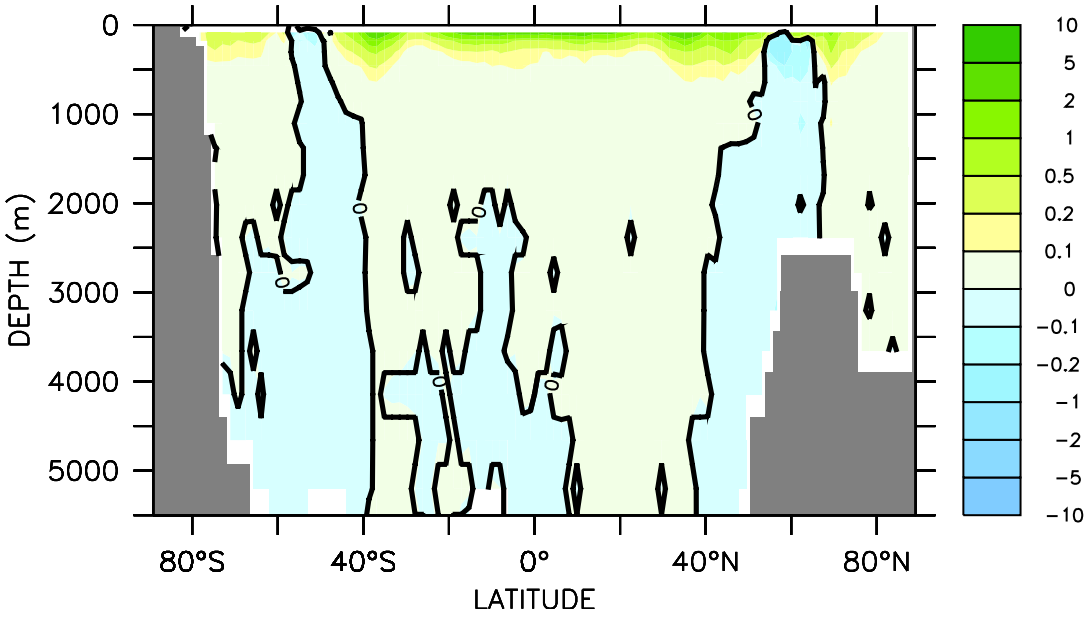

Figure S5: Zonally integrated difference in respiratory oxygen consumption, year 2650 minus year 2020. Units are mmol O_2 m^{-3} yr^{-1}.

Figures

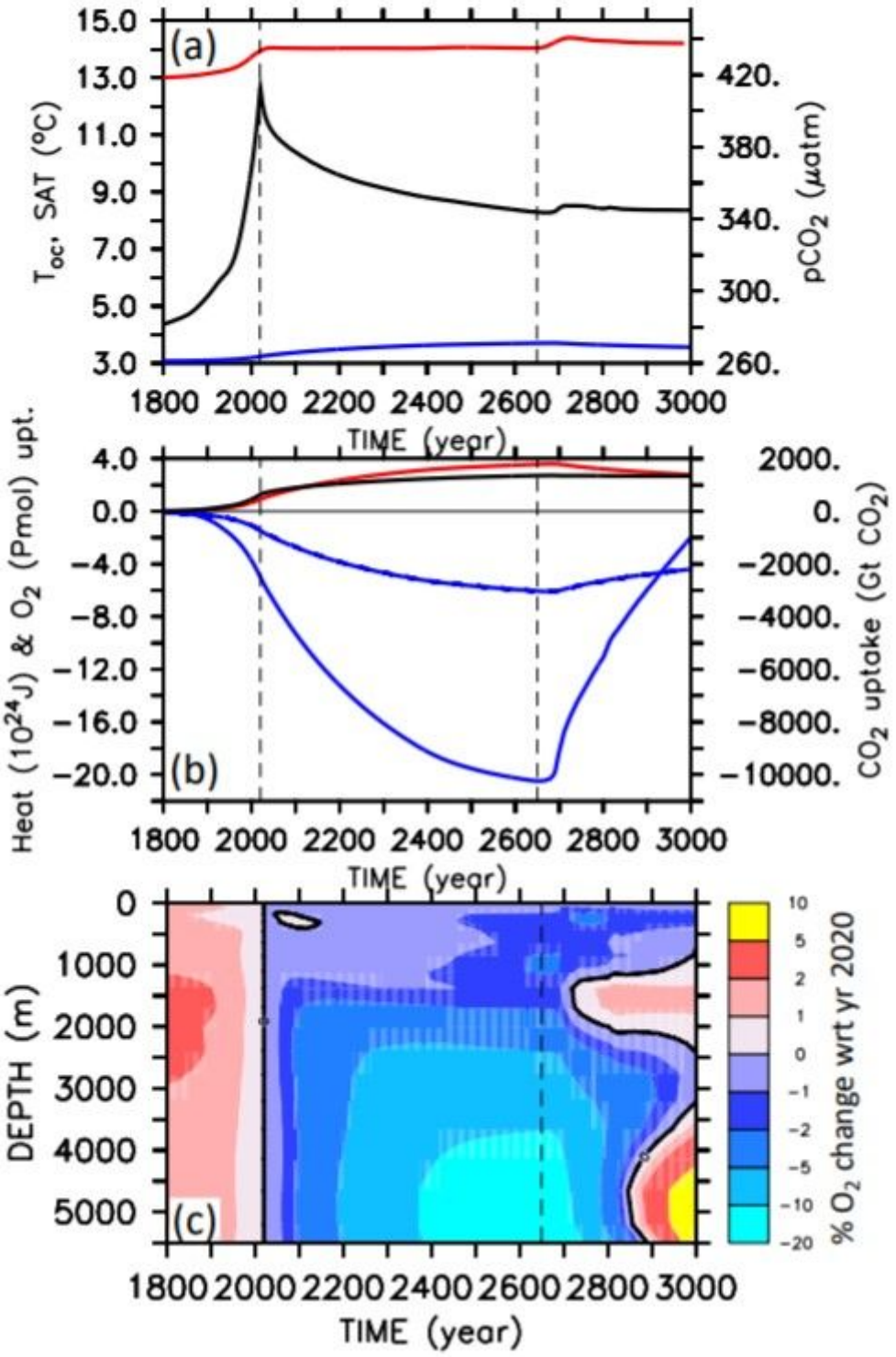

Figure 1

(a) Simulated global annual-mean surface air temperature (SAT, red), atmospheric pCO2 (black) and ocean mean temperature (Toc, blue). (b) Change in ocean inventory of heat (red), CO2 (black), dissolved oxygen (O2, blue) and its abiotic (solubility) component (abiotO2, dashed blue) with respect to year 1800.

% O2 change wrt yr 2020 (c) Change in laterally integrated oxygen concentration as a function of depth over time, expressed in percent change relative to year 2020. Vertical dashed black lines mark then end of year 2020 when emissions stop and the end of the evaluation period in year 2650, just before the onset of the Southern Ocean deep convection event.

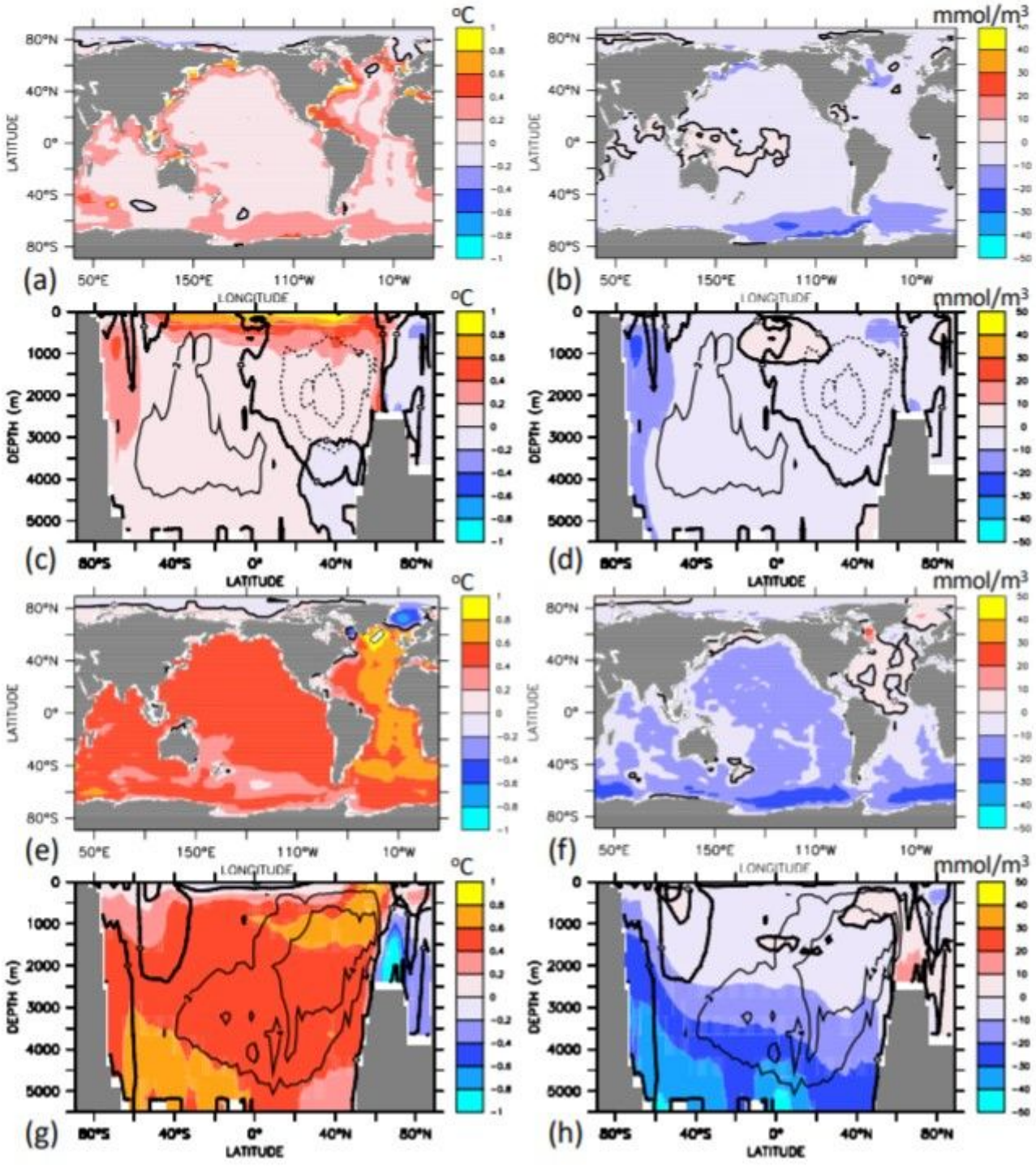

Figure 2

Simulated change in temperature (left column) and oxygen (right column). (a,b) vertically averaged difference year 2020 minus 1800, (c,d) zonally averaged year 2020 minus year 1800, (e,f) vertically averaged difference year 2650 minus 2020, and (g,h) zonally averaged difference year 2650 minus 2020. Contour lines indicate changes in the zonally averaged overturning stream function, with 2 Sv spacing of the iso-contours.

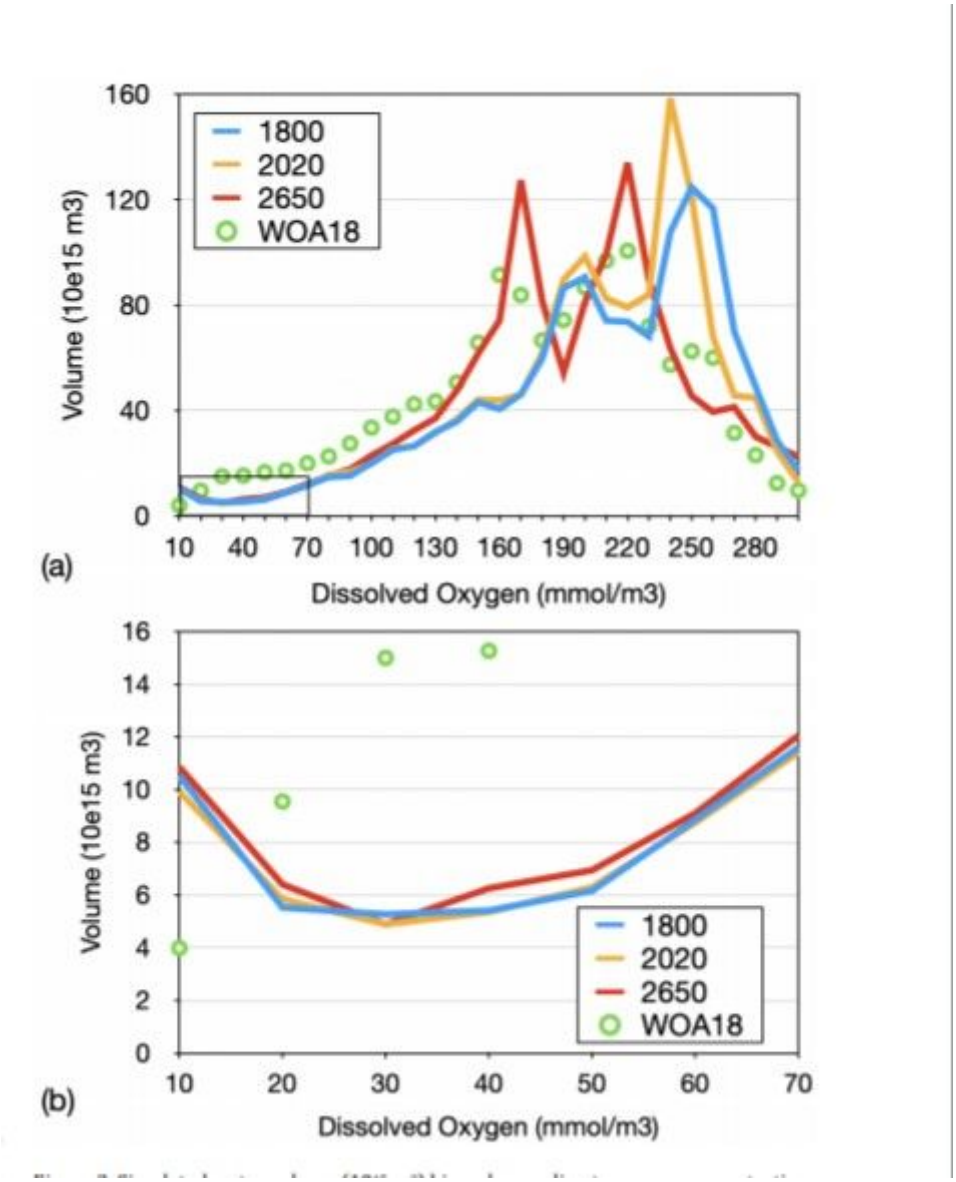

Figure 3

Simulated water volume (1015 m3 455) binned according to oxygen concentration with bin width of 10 mmol m-3 456 . Blue refers to year 1800, orange to year 2020 and red to year 2650. Circles refer to the data of the World Ocean Atlas 2018 (ref.24)

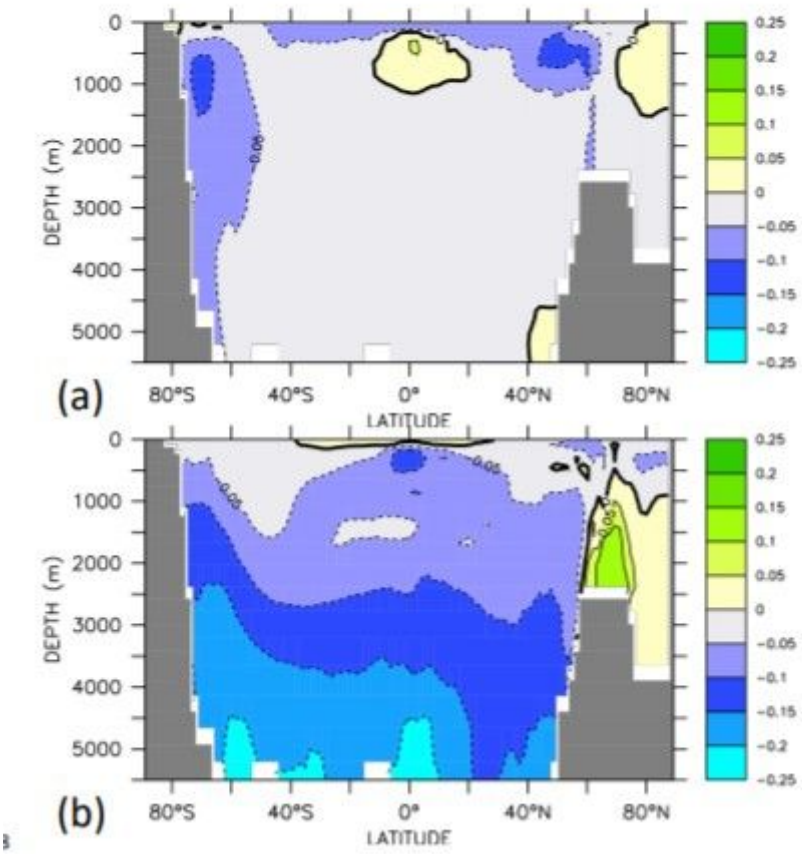

Figure 4

Zonally averaged relative changes in the metabolic index F (see text) for (a) year 2020 with respect to year 1800, (b) year 2650 with respect to year 2020.

Supplementary Files

This is a list of supplementary files associated with this preprint. Click to download.

- s1.jpg
- s2.jpg
- s3.jpg
- s4.jpg
- s5.jpg